Analytica Chimica Acta 1089 (2019) 152–164

Contents lists available at ScienceDirect

Analytica Chimica Acta

journal homepage: www.elsevier.com/locate/aca

A highly selective and sensitive detection of insulin with chemiluminescence biosensor based on aptamer and oligonucleotide-AuNPs functionalized nanosilica @ graphene oxide aerogel

Yuanling Sun, Yanna Lin, Weiyan Sun, Rui Han, Chuannan Luo*, Xueying Wang**, Qin Wei

Key Laboratory of Interfacial Reaction & Sensing Analysis in Universities of Shandong, School of Chemistry and Chemical Engineering, University of Jinan, Jinan, 250022, PR China

HIGHLIGHTS

- Multi-functioned silica @ graphene oxide aerogel composite was successfully prepared.
- Aptamer was introduced to improve the selectivity of the biosensor.
- Oligonucleotide-gold nanoparticle improved the sensitivity of the biosensor.
- The CL biosensor was successfully used for insulin injection samples.

GRAPHICAL ABSTRACT

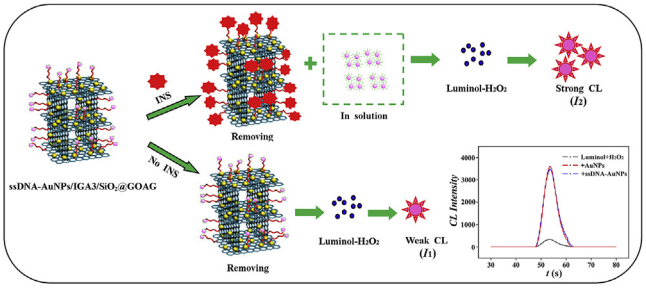

ARTICLE INFO

Article history:
Received 10 April 2019
Received in revised form
20 August 2019
Accepted 2 September 2019
Available online 3 September 2019

Keywords:
Chemiluminescence
Insulin
Graphene oxide aerogel
Aptamer
Gold nanoparticles

ABSTRACT

A novel, highly selective and sensitive chemiluminescence (CL) biosensor for insulin (INS) detection was proposed based on aptamer and oligonucleotide-gold nanoparticles functionalized nanosilica @ graphene oxide aerogel. Initially, nanosilica functionalized graphene oxide aerogel (SiO_2@GOAG) was successfully prepared and the composite showed rich pore distribution, large specific surface area and good biocompatibility. Insulin aptamer (IGA3) was used as a biorecognition element and oligonucleotide functionalized gold nanoparticles (ssDNA-AuNPs) was used as CL signal amplification materials, which were functionalized on the surface of SiO_2@GOAG. The multi-functionalized composite - ssDNA-AuNPs/IGA3/SiO_2@ GOAG was obtained and used to construct the CL biosensor for insulin detection. When insulin is present in a sample, the insulin will bind to the IGA3, which will result in the release of ssDNA-AuNPs. The released ssDNA-AuNPs would catalyze the luminescence of luminol and H_2O_2. The linear range of the CL biosensor for insulin detection was 7.5×10^{-12} to 5.0×10^{-9} moL/L and the detection limit was 1.6×10^{-12} moL/L (S/N = 3). The selectivity and stability of the CL biosensor were also studied and the results showed that the biosensor exhibited high selectivity and good stability due to the introduction of ssDNA-AuNPs/IGA3/SiO_2@GOAG. The CL biosensor was finally used for recombinant human insulin detection in recombinant human insulin injection and the results were satisfactory.

* Corresponding author.
** Corresponding author.
E-mail addresses: chm_yfl518@163.com (C. Luo), chm_wangxy@ujn.edu.cn (X. Wang).

https://doi.org/10.1016/j.aca.2019.09.004
0003-2670/

1. Introduction

Diabetes is a chronic or metabolic disease caused by the high blood glucose level in the circulatory system [1]. Both hyperglycaemia (high blood glucose levels) and hypoglycaemia (low blood glucose levels) can cause human health issues. Hyperglycaemia can cause long-term damage, rupture, and failure of various organs, especially the eyes, kidneys, nerves, heart and veins, while hypoglycemia can cause sweating, hunger, palpitation, trembling, paleness and can also be insufficiency, irritability, irritability and even coma [2]. Insulin is first synthesized as preproinsulin in the β cells of the pancreas islets and human insulin are secreted by the β cells after a series of conversions [3]. As the only hormone to lower blood glucose in the body, insulin can promotes the synthesis of glycogen, adipose and protein. Diabetes occurs if the insulin in the body is insufficient for a long time [4,5]. Exogenous insulin is mainly used for the treatment of diabetes. There are many kinds of insulin used in clinical practice, such as insulin aspart, insulin lispro, biosynthetic human insulin, low-protamine zinc insulin, and insulin glargine. Although glucose meters have been relatively effective at detecting glucose, and enable subsequent determination of insulin levels, there is still a problem in developing a commercial Point-of-Care device that directly measures free insulin. Solving the problem is significant because modern models use insulin doses to control blood glucose levels - based on estimates of insulin-related glucose uptake [6,7]. Therefore, the determination of insulin is extremely important in fields of biomedicine and clinical diabetes treatment. There are various methods to detect insulin [8], including electrochemistry sensor [9,10], electrochemiluminescence sensor [11], fluorescence sensor [12], liquid chromatography-mass spectrometry (LC-MS/MS) [13], surface enhanced raman scattering (SERS) [14] and immunoassay sensor [15,16]. However, some of these methods are hindered by time-consuming operation, low sensitivity, expensive or cumbersome instruments, which limit their further application. So there is an urgent need to find a simple, low-cost, highly selective, sensitive and accurate method to detect insulin. Chemiluminescence (CL) has attracted widespread researchers' attention owning to its high sensitivity, wide linear range, fast analysis speed, simple operation, no pollution to environment, and ease of use with other devices [17]. There are rare reports about insulin detection by CL method [18,19]. Yao et al. developed a microfluidic-based detection system for the rapid determination of insulin through a CL immunoassay [18]. A novel CL biosensor based on resonance energy transfer was developed for sensitive determination of insulin [19].

Chemiluminescence (CL) is a detection method based on CL reactions. Its excitation energy is supplied by the reaction itself, so the background interference is eliminated effectively. For CL reactions, intermediates generated in the process of electron excitation are unstable and the CL signal occurs when intermediates return to the ground state [20]. However, one disadvantage of the CL method is its poor selectivity because the CL intensity easily changed when there are coexisting substances in sample. But the deficiency is overcome by introducing some biorecognition materials including antibodies complex [21], aptamer composites [22,23] and molecularly imprinted polymers [24]. Among these, aptamer composites show excellent properties of the easy synthesis, good stability, and a range of aptamers [25,26]. For example, Wu et al. prepared a CL biosensor for glycoprotein tenascin-C determination based on aptamers labeled with N-(4-aminobutyl)-N-ethylisoluminol (ABEI) [27]. Lin et al. developed a selective vascular endothelial growth factor (VEGF165) CL biosensor based on two specific aptamers sequences [28]. Another disadvantage is the weak CL intensity due to the low quantum yield of inorganic molecules [29]. Therefore, the catalysts or signal-amplified materials are necessary to construct CL biosensors. Metal porphyrins [30], metal nanoparticles [31], quantum dots [32], peroxidases or peroxide mimic enzymes [33,34] are common catalysts in CL detection. As a metal nanoparticle, gold nanoparticles (AuNPs) has been widely used in CL systems compared with other catalysts. Zhang et al. found that AuNPs with different sizes could improve the CL intensity of luminol-H_2O_2 at some extent [35]. Li et al. proposed that AuNPs could trigger the CL reaction of luminol-$AgNO_3$, and some biological reducing compounds including monoamine neurotransmitters and their metabolites, reductive amino acids, ascorbic acid, uric acid, and glutathione showed a significant inhibitory effect on the luminescence intensity [36]. Zhang et al. prepared a CL biosensor for sensitive detection of fibrillar fibrin based on AuNPs catalyzing luminol-H_2O_2 [37].

Two-dimensional (2D) graphene materials are often used as support materials in biosensors owing to their excellent surface properties of good electrical conductivity, electrical conductivity, mechanical properties and large specific surface area [38]. However, their further applications were limited due to their easy to aggregation and agglomeration. Three-dimensional (3D) graphene materials have overcome the above-mentioned drawbacks. 3D graphene with porous structure includes graphene foam, sponge, aerogel and hydrogel. Among these materials, graphene aerogel has attracted researchers' great interest owing to its easy synthesis, high elasticity and strong adsorption capacity. Chen et al. prepared a porous graphene-based aerogel (GAs) by cysteamine as a cross-linking agent and GAs presented good adsorption property for common dyes [39]. Wang et al. prepared a Fe_3O_4 nanoparticle/graphene aerogel (Fe_3O_4/GA) through a simple liquid phase precipitation method and applied it to an anode material in lithium ion battery, and the aerogel exhibited excellent lithium storage performance [40]. Li et al. prepared spheroidal graphene aerogel modified with both folic acid and octadecylamine, and the aerogel was also applied to construct electrochemical sensors for cancer cells detection [41].

Nanosilica (SiO_2) is a non-toxic, odorless and eco-friendly inorganic non-metallic material. Similarly to other nanomaterials, SiO_2 exhibits many special properties when its size changes from micron to nanometer, such as its large specific surface area, good stability, good dispersion, easily modified surface and excellent biocompatibility. Therefore, SiO_2 has been widely used in fields of food production, industrial coatings, optics semiconductors, biochemistry and medicine [42–45], especially in biosensors. Wang et al. synthesized phytic acid functionalized silica nanoparticles and applied it to construct a sensitive biosensor for dopamine detection [46]. Chen et al. prepared mesoporous silica (MSN) and used it to a controlled release system, and a highly sensitive CL biosensor for cocaine detection was realized [47]. Zhu et al. prepared a mesoporous silica coated gold nanorods fluorescent probe (Au@SiO_2) and achieved simple and sensitive detection of bovine serum albumin (BSA) [48].

In our work, multifunctional ssDNA-AuNPs/IGA3/SiO_2@GOAG was successfully synthesized, in which SiO_2@GOAG had rich pore distribution, large specific surface area and good biocompatibility, insulin aptamer (IGA3) first reported by Yoshida et al. [49] was used as a bioreceptor for target recognition and ssDNA-AuNPs as a catalytic material for signal amplification. The composite was then applied to the construction of CL biosensor for insulin detection. When insulin is present in a sample, the insulin will bind to the IGA3, which will result in the release of ssDNA-AuNPs. After the removal of INS@IGA3/SiO_2@GOAG, released ssDNA-AuNPs would catalyze the CL reaction of luminol-H_2O_2. So the novel, highly selective and sensitive CL biosensor was successfully prepared for insulin detection.

2. Experimental

2.1. Chemicals and reagents

Graphite powder was purchased from Tianjin Hongyan Chemical Reagent Co., Ltd. Ethyl orthosilicate (TEOS), aminopropyltriethoxysilane (APTS), anhydrous toluene, chloroauric acid and sodium citrate were purchased from Shanghai Aladdin Biochemical Technology Co., Ltd. Luminol and polyvinyl alcohol 1788 (PVA 1788) was purchased from Shanghai Maclean Biochemical Technology Co., Ltd. Adrenaline (Adr) was purchased from Tianjin Damao Chemical Reagent Factory. Recombinant human insulin standard (insulin, INS, 11061-68-0) was purchased from Beijing Bayer Biotech Co., Ltd and recombinant human insulin injection (40 IU/mL, S20030075) was purchased from Jiangsu Wanbang Biochemical Pharmaceutical Group Co., Ltd. Bovine serum albumin (BSA), cystine (Cys) and other biological interference substances were purchased from Beijing Bayer Biotech Co., Ltd. Potassium permanganate ($KMnO_4$), hydrogen peroxide (H_2O_2), sodium hydroxide (NaOH) and all other chemicals or reagents unless otherwise stated were all analytical reagent grade. Oligonucleotide DNA chain sequences were purchased from Shanghai Sangon Biotech Co. Ltd and these sequences were as follows: insulin aptamer (IGA3): 5' - GGTGGTGGGGGGGGTTGGTAGGGTGTCTTC - 3′, complementary DNA (ssDNA): 5' - CCCCCCACCACC–$(CH_2)_3$–SH - 3′ and nonspecific aptamer (N-Apt): 5' - GGTGGTGGGGGGCCAACCATCGGTGTCTTC - 3'. Samples in whole experiments were prepared by 0.02 moL/L phosphate buffer solution (PBS, pH = 7.4). Other solutions used in this work were prepared by ultra-pure water.

2.2. Instruments

The morphologies of prepared composites were characterized by a scanning electron microscope (SEM, GUANTA FEG 250, FEI, America) or a transmission electron microscopy (TEM, JEOL1400, Japan). The fourier transform infrared spectroscopy measurement (FTIR, PerkinElmer Corporation, America) was used to measure special functional groups. The X-ray powder diffraction characterization was made on a D8 focus spectrometer (XRD, Brooke AXS, Germany). Ultraviolet–visible spectrophotometer (UV–Vis, UV-2550, China) and fluorescence spectrophotometer (FL, Shimadzu RF-5301, Japan) were used to characterize AuNPs. The specific surface area and pore size were determined by Brunauer-Emmett-Teller surface area measurement (BET, Quantachrome, America). The CL signal was determined by an IFFM-E flow injection CL analyzer (Remex Electronic instrument High-Tech Ltd, China) that equipped with an automatic injection system and a detection system.

2.3. Preparation of GO

GO was synthesized by a modified Hummers' method as mentioned in our previous work [50]. Briefly, 0.5 g graphite powder was added to 100 mL mixed acid (V_{H2SO4}:V_{HNO3} = 9:1) in a 250 mL flask. After that, 3.0 g $KMnO_4$ was added to the flask and stirred for 12 h at 90 °C. Then, 30% H_2O_2 was slowly added until no reaction occurred. After centrifugal separation, 0.2 moL/L HCl and water were used to wash the product. Final product was obtained after vacuum drying at 60 °C.

2.4. Preparation of SiO_2 microspheres

SiO_2 microspheres were synthesized by a modified stober method [51]. 2.5 mL ammonia and 1.0 mL TEOS were added to 20 mL mixed solvent ($V_{ethanol}$:V_{water} = 9:1) under magnetic stirring at 400 r/min. Then, the mixture was stirred for 12 h at 10 °C. The product was collected by centrifugation and vacuum drying at 60 °C.

2.5. Preparation of SiO_2@GOAG

0.5 g SiO_2 was dispersed to 25 mL mixture (V_{APTS}:$V_{toluene}$ = 1:5) in a 50 mL flask. Under N_2, the mixture was reflux heated for 12 h at 110 °C. After centrifugation, the product was washed by water and vacuum dried at 50 C. So the aminated SiO_2 (SiO_2–NH_2) was obtained. 0.5 g SiO_2–NH_2 and 0.1 g SDS were added to 50 mL 6.0 mg/mL GO dispersion. The excess moisture of the dispersion was removed by rotary evaporation and final 3% (wt) dispersion was obtained. 0.5 g PVA-1788 was dissolved to 17 mL water at 90 °C. Then the 3% dispersion was slowly added to the dissolved PVA-1788 to obtain uniform slurry. After freeze drying, SiO_2@GOAG was obtained.

2.6. Preparation of ssDNA-AuNPs

AuNPs was prepared by the reduction of chloroauric acid. 3.65×10^{-5} mol chloroauric acid was diluted to 100 mL water and the solution was heated until bubbled slightly. 3.0 mL 1% (wt) of sodium citrate was added to the boiling chloroauric acid and reacted until the color of solution changed to burgundy. Then the reaction mixture was stirred to room temperature to obtain AuNPs sol and stored at 4 °C for use.

100 μL AuNPs sol was added to 10 mL 4.0×10^{-8} moL/L of ssDNA and shaken for 12 h to mix. Then, the mixture was incubated for 12 h at 25 °C. After that, the mixture was centrifuged at 10000 r/min by a desktop high-speed centrifuge (TG16-WS, Hunan Xiangyi Centrifuge Instrument Co., Ltd.) to remove the excess ssDNA. The product was transferred to a 10 mL centrifuge tube and stored at 4 °C for later use.

2.7. Preparation and properties study of IGA3/SiO_2@GOAG

IGA3/SiO_2@GOAG was prepared by modifying IGA3 on the surface of SiO_2@GOAG through the non-covalent interaction such as π-π stacking effect and hydrogen bonding between IGA3 and SiO_2@GOAG, as mentioned in literatures [52–54]. The saturated immobilization capacity was measured by the following procedures. IGA3 with different concentrations (3.0×10^{-9}, 3.5×10^{-9}, 4.0×10^{-9}, 4.5×10^{-9}, 5.0×10^{-9}, 5.3×10^{-9}, 5.5×10^{-9}, 5.8×10^{-9} and 6.0×10^{-9} moL/L) were added to 25 mL colorimetric tubes preplaced with 0.01 g SiO_2@GOAG. These tubes were shaken for 1 h by a constant temperature oscillator at 25 °C. SiO_2@GOAG appeared as a visible rod-like structure (Fig. S1), so it could be separated from the solution by tweezers. After separation, the CL intensity of solution in these tubes was detected by the CL analyzer. The saturated immobilization capacity was calculated by the mutation point of CL signal and the formula was as follows:

$$Q_e = \frac{c_e \times V}{m} \quad (1)$$

of which Q_e (mol/g) was the saturated immobilization capacity of per unit mass of SiO_2@GOAG to IGA3; c_e (mol/L) was the concentration of IGA3 at the CL signal mutation point; V (L) was the volume of IGA3 and m (g) was the addition mass of SiO_2@GOAG.

2.8. Preparation and properties study of ssDNA-AuNPs/IGA3/SiO_2@GOAG

The multi-functioned ssDNA-AuNPs/IGA3/SiO_2@GOAG was

prepared by connecting ssDNA-AuNPs on the surface of IGA3/SiO_2@GOAG through the base complementary pairing effect of ssDNA and IGA3. Similar to the saturated immobilization capacity of SiO_2@GOAG to IGA3, the effective combination capacity of IGA3/SiO_2@GOAG to ssDNA-AuNPs was measured by the following procedures. Different concentrations of ssDNA-AuNPs (1.6×10^{-9}, 1.8×10^{-9}, 2.0×10^{-9}, 3.0×10^{-9}, 4.0×10^{-9}, 5.0×10^{-9}, 5.25×10^{-9}, 5.5×10^{-9}, 5.75×10^{-9} and 6.0×10^{-9} moL/L) were added to 25 mL colorimetric tubes pre-placed with 0.01 g IGA3/SiO_2@GOAG. These tubes were shaken for 1 h by a constant temperature oscillator at 25 °C. After separation by tweezers, the CL intensity of solution in these tubes was detected by the CL analyzer. The saturated immobilization capacity was calculated by the mutation point of CL signal and the formula was as follows:

$$Q_e' = \frac{c_e \times V'}{m'} \quad (2)$$

of which Q_e' (mol/g) was the saturated combination capacity of per unit mass of IGA3/SiO_2@GOAG to ssDNA-AuNPs; c_e' (mol/L) was the concentration of ssDNA-AuNPs at the CL signal mutation point; V' (L) was the volume of ssDNA-AuNPs and m' (g) was the addition mass of IGA3/SiO_2@GOAG.

The synthesis of ssDNA-AuNPs/IGA3/SiO_2@GOAG was shown in Fig. 1(A).

2.9. Samples detection procedures

The detection procedures of insulin are as followed and shown in Fig. 1(B). When insulin is absence, the CL intensity (I_1) is low and equivalent to the CL intensity (I_0) of blank control group (PBS buffer). When insulin is presence, insulin and IGA3 are recognized and bound together to form INS/IGA3/SiO_2@GOAG, making ssDNA-AuNPs release from the surface of IGA3/SiO_2@GOAG. The released ssDNA-AuNPs catalyzes the reaction of luminol-H_2O_2 and a significantly enhanced CL signal (I_2) is obtained. The final $\Delta I = I_2 - I_0$ is used to quantitative detection of insulin.

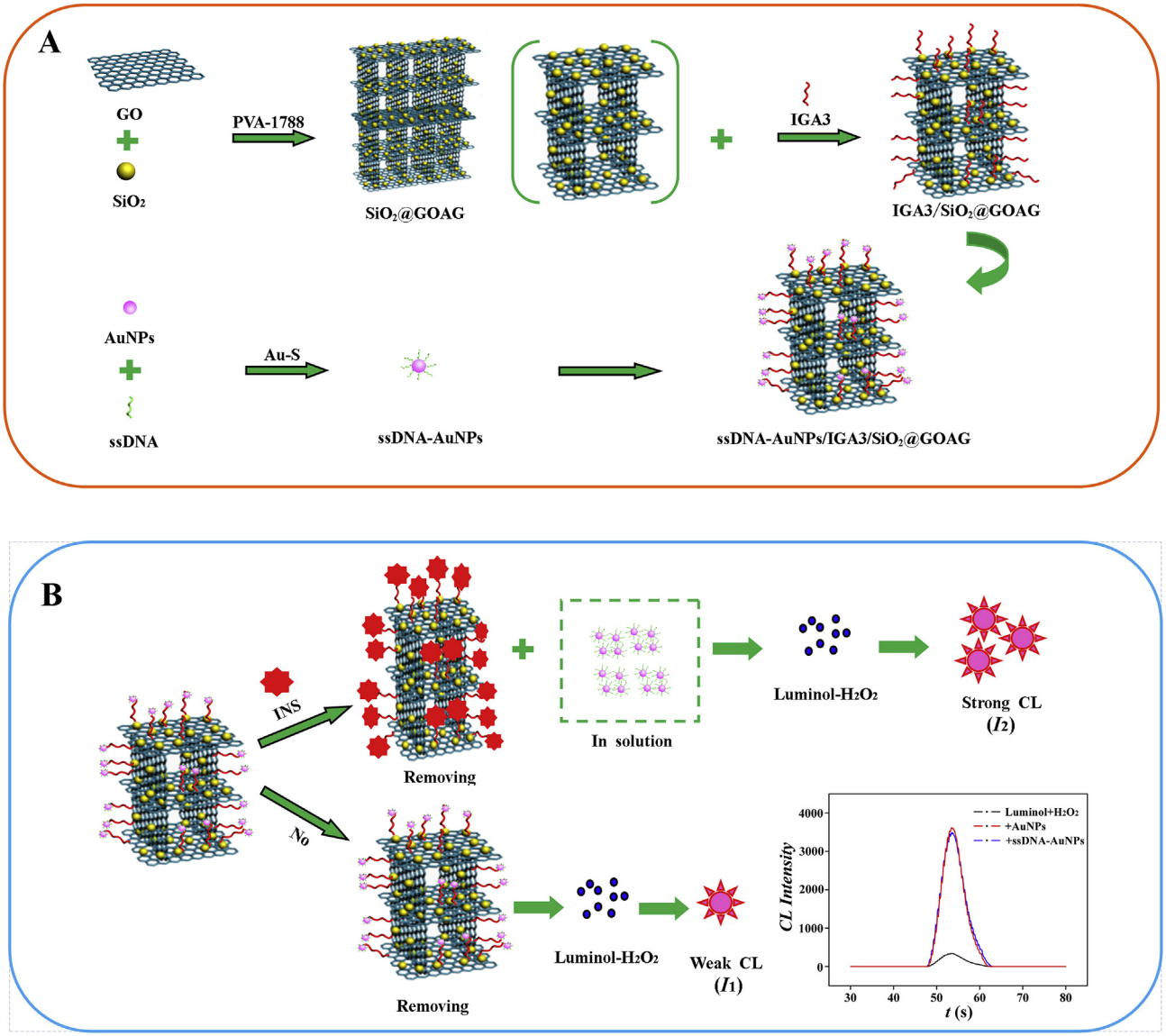

Fig. 1. The preparation of ssDNA-AuNPs/IGA3/SiO_2@GOAG (A) and the construction principles of the CL biosensor for insulin detection (B).

3. Results and discussion

3.1. Characterizations

The SEM characterizations of GO, SiO_2 and SiO_2@GOAG were showed in Fig. 2. 5.00 KV of acceleration voltage was used for SEM characterization. The sample preparation for SEM test was shown as follows. Firstly, the carbon double-sided conductive adhesive (8 mm, NEM) was bonded to the sample holder. Then, the powder sample was evenly sprinkled on the holder and the non-stick powder was blown off by a rubber suction bulb. Finally, a conductive film was coated on the sample for observation. GO exhibited a layered structure with more wrinkles on its surface in Fig. 2(A), which provided a larger specific surface area for the immobilization of IGA3. In Fig. 2(B), SiO_2 appeared a relatively regular spherical. Fig. 2(C and D) showed the SiO_2 microspheres were successfully coated on the aerogel.

Subsequently, FTIR characterizations of GO, SiO_2, SiO_2—NH_2 and SiO_2@GOAG were carried out. In Fig. 3(A), the peaks at 1380 and 1055 cm^{-1} were the deformation vibration peak of —OH and the stretching vibration peak of C—O, respectively, and these characteristic peaks indicated that GO with different oxygen-containing functional groups was successfully synthesized. For SiO_2, the absorption peak at 950 cm^{-1} was attributed to the stretching vibration of Si—O and the peak at 805 cm^{-1} was due to the stretching vibration of Si—O—Si, and these peaks showed the successful synthesis of SiO_2. For SiO_2—NH_2, a characteristic peak of —NH_2 appeared at 3040 cm^{-1}. For SiO_2@GOAG, these characteristic peaks of GO and SiO_2 appeared, which further indicated the successful synthesis of SiO_2@GOAG.

The XRD characterization curves of GO, SiO_2 and SiO_2@GOAG were shown in Fig. 3(B). The peak around 11.5° was the characteristic peak of GO [55]. The broad and wide characteristic peak around 25.0° was attributed to the characteristic peak of SiO_2 [56]. The above-mentioned characteristic peaks were all appeared in the curve of SiO_2@GOAG and indicated that SiO_2@GOAG was successfully prepared. The BET characterization of SiO_2@GOAG was also obtained and the results were shown in Fig. 3(C and D). The specific surface area of SiO_2@GOAG was 292.31 m^2/g and the distribution of pore size was around 4.63 nm. It illustrated SiO_2@GOAG had a large specific surface area and a dense pore-like distribution.

The characterizations of ssDNA-AuNPs were performed to support its successful preparation. The TEM characterizations were shown in Fig. 4(A and B). The particle size of AuNPs was around 8 nm. AuNPs had obvious aggregation while ssDNA-AuNPs had the relatively uniform dispersion. The FL and UV curves of AuNPs were seen in Fig. 4(C).

The FL absorption peak at 415 nm was the characteristic of AuNPs when the excitation wavelength is 362 nm and the UV absorption peak at 530 nm was the characteristic of AuNPs, which clarified AuNPs was successfully synthesized. Fig. 4(D) was the UV curves of ssDNA, AuNPs and ssDNA-AuNPs to illustrate the successful synthesis of ssDNA-AuNPs. The peaks at 260 nm and 530 nm were characteristic absorption peaks of ssDNA and AuNPs, respectively. The characteristic peak at 260 nm of ssDNA-AuNPs exhibited a slight red shift, which might due to the formation of the Au—S bond [57].

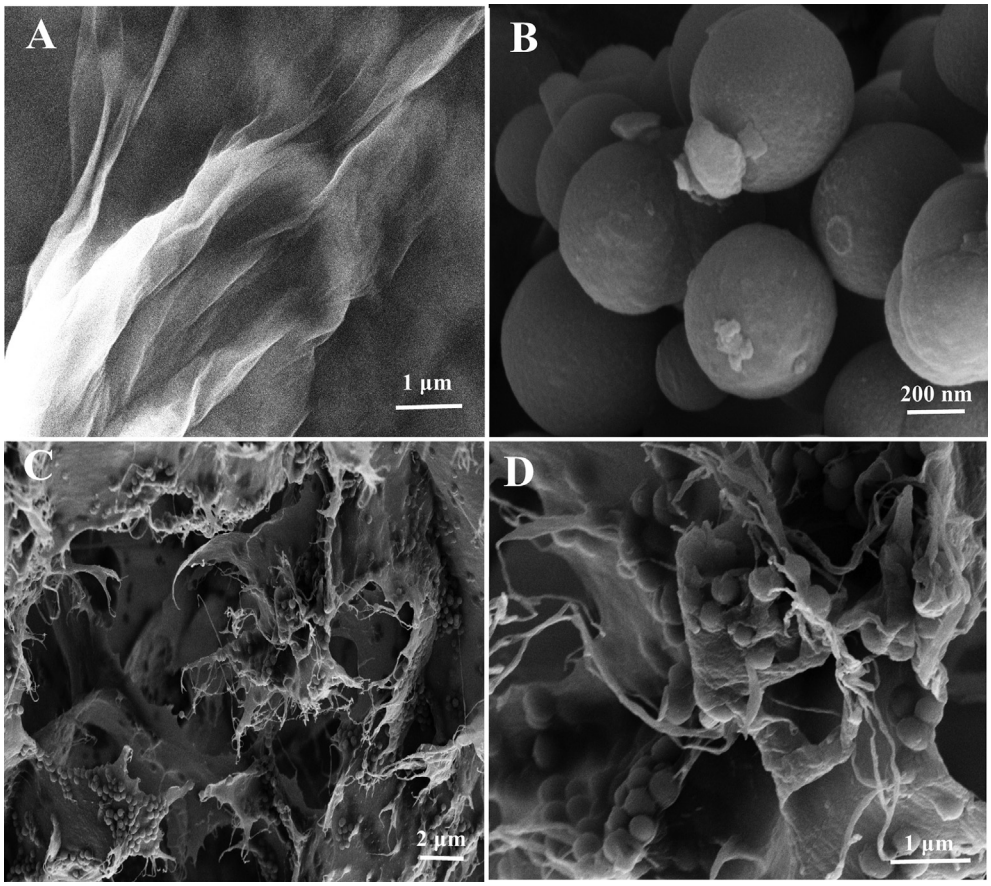

Fig. 2. The SEM images of GO (A), SiO_2 (B) and SiO_2@GOAG (C, D).

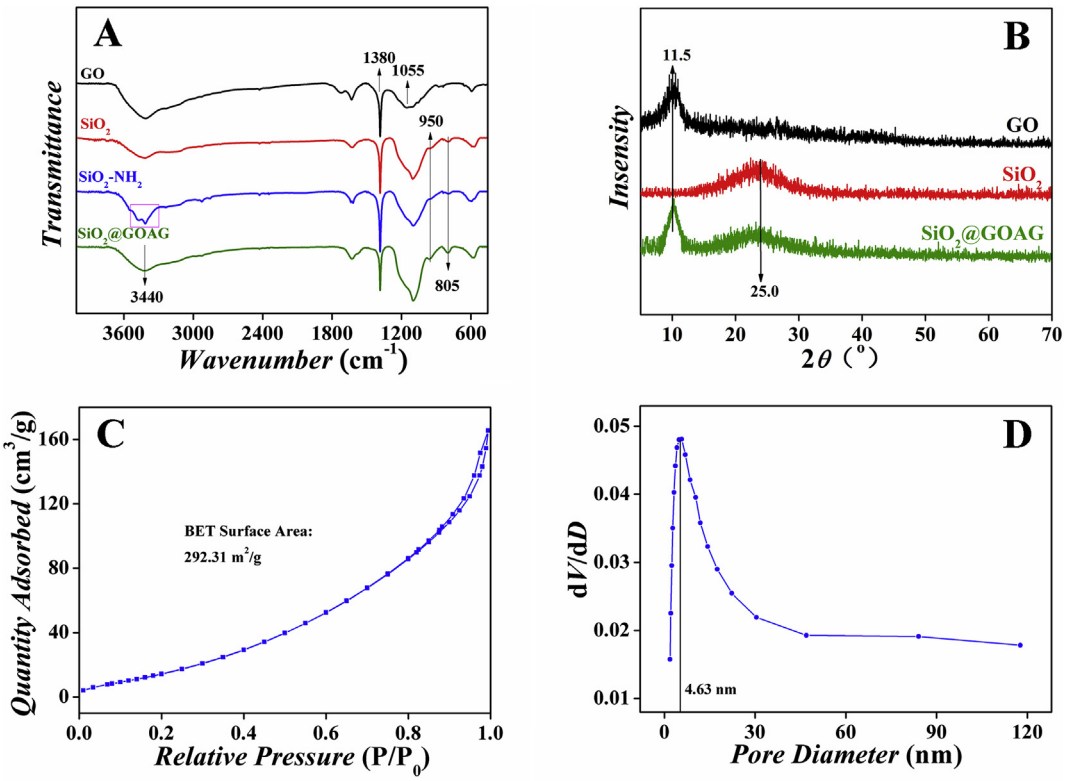

Fig. 3. The FTIR curves of GO, SiO_2, SiO_2—NH_2 and SiO_2@GOAG (A); the XRD curves of GO, SiO_2 and SiO_2@GOAG (B); the BET characterizations of SiO_2@GOAG (C, D).

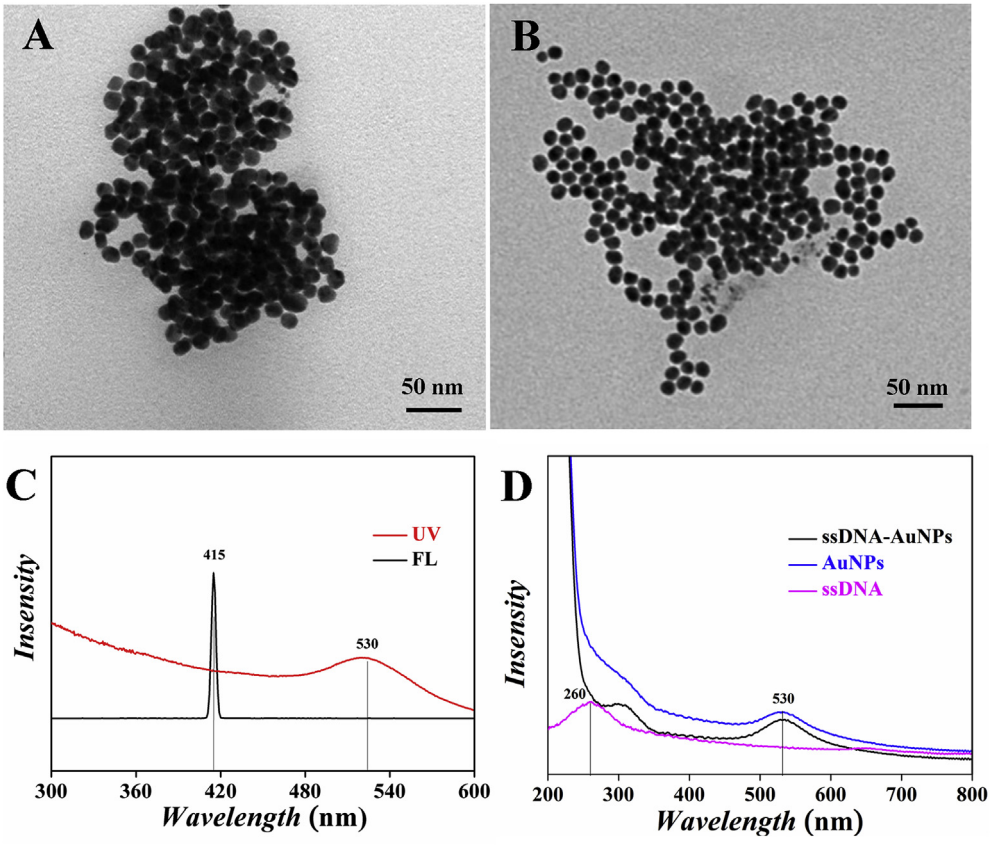

Fig. 4. The TEM images of AuNPs (A) and ssDNA-AuNPs (C); the UV and FL curves of AuNPs (B); the UV curves of AuNPs, ssDNA and ssDNA-AuNPs (D).

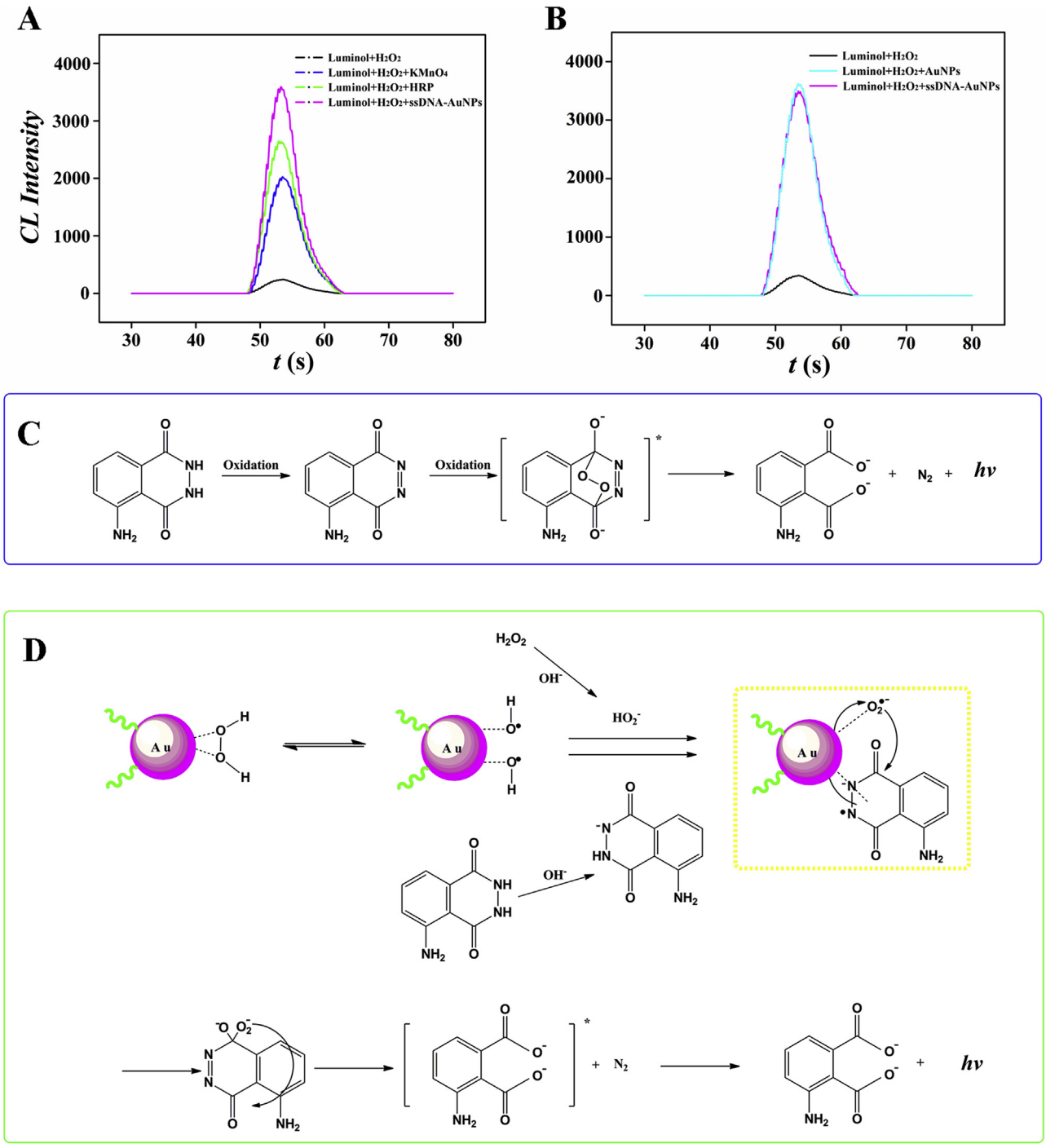

Fig. 5. Different CL intensity of luminol-H_2O_2 with different catalysts, conditions: 5.0×10^{-5} moL/L luminol, 0.10 moL/L H_2O_2, 5.0×10^{-6} moL/L $KMnO_4$, 1.0×10^{-8} moL/L HRP and 2.5×10^{-8} moL/L ssDNA-AuNPs (A); different CL intensity in the presence of no catalyst, AuNPs and ssDNA-AuNPs, conditions: 5.0×10^{-5} moL/L luminol, 0.10 moL/L H_2O_2, 2.5×10^{-8} moL/L AuNPs and 2.5×10^{-8} moL/L ssDNA-AuNPs (B); generally accepted schematic diagram of luminol luminescence (C); the schematic diagram of ssDNA-AuNPs catalyzing luminol-H_2O_2 (D).

3.2. Construction principles and catalytic mechanism study

Construction principles of the proposed CL biosensor were illustrated as follows and showed in Fig. 1(B). When insulin is present in a sample, the insulin will bind to the IGA3, which will result in the release of ssDNA-AuNPs. After that, INS@IGA3/SiO_2@GOAG is easily separated by a tweezer and released ssDNA-AuNPs can catalyze the CL reaction of luminol-H_2O_2 and realize the quantitative detection of insulin.

The ability of ssDNA-AuNPs catalyzing luminol-H_2O_2 was also researched. As shown in Fig. 5(A), the CL curves of different catalysts to catalyze luminol-H_2O_2 were researched and these catalysts contained $KMnO_4$ (5.0×10^{-6} moL/L), horseradish peroxidase (HRP, 1.0×10^{-8} moL/L) and ssDNA-AuNPs (2.5×10^{-8} moL/L). The CL intensity of ssDNA-AuNPs was significantly stronger than that of higher concentrations of $KMnO_4$ and HRP. For example, the CL

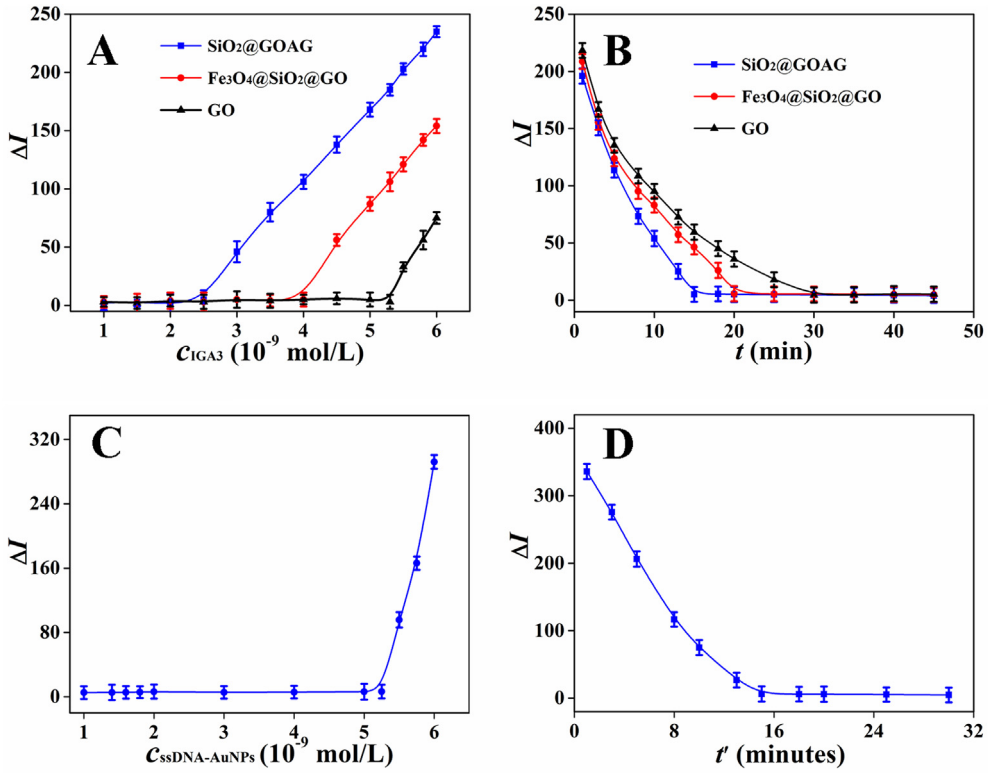

Fig. 6. The saturated immobilization amount curves (A) and equilibrium time curves (B) of SiO_2@GOAG to IGA3; combination amount curve (C) and equilibrium time (D) of IGA3/SiO_2@GOAG to ssDNA-AuNPs (Error bar of all graphs: $n = 6$).

intensity of ssDNA-AuNPs was 1.25 times that of HRP at a concentration higher than 2.5 times.

At the same time, the feasibility of the CL biosensor was studied. As shown in Fig. 5(B), although the catalytic ability of ssDNA-AuNPs to Luminol-H_2O_2 was somewhat attenuated, the CL intensity catalyzed by ssDNA-AuNPs was still strong, which was consistent with previously reported articles [35,37,58]. Single-stranded DNA could attenuate the aggregation of AuNPs and aggregated AuNPs showed a stronger ability than dispersed AuNPs to catalyze the reaction of Luminlo-H_2O_2.

It is generally known that luminol can be oxidized to produce luminescence. As shown in Fig. 5(C), the luminol molecule produces an unstable luminol intermediate after multiple oxidations. Intermediates release energy and emit luminescence when they return to the ground state. The possible mechanisms of ssDNA-AuNPs catalyzing luminol-H_2O_2 were shown in Fig. 5(D). Under alkaline conditions, luminol and H_2O_2 generate negative ions, and the intermediate (ssDNA-AuNPs ··· H_2O_2) is generated. The formation of luminol at transition state is promoted in the presence of the above two negative ions and promotes the CL reaction. The possible catalytic mechanisms of ssDNA-AuNPs catalyzing luminol-H_2O_2 described above were consistent with the reported literature [35,59].

3.3. Immobilization properties

The immobilization properties of SiO_2@GOAG to IGA3 were researched, including the saturated immobilization amount (immobilization isotherms) and immobilization equilibrium time (immobilization kinetics). To illustrate the better immobilization abilities of SiO_2@GOAG, the immobilization properties of GO and Fe_3O_4@SiO_2@GO were also researched at the same experimental conditions. Fe_3O_4@SiO_2@GO was prepared by our previous work [60]. Fig. 6(A) was the saturated immobilization amount curves of different materials to IGA3. It showed that IGA3 with different concentrations caused different changes of CL signal intensity. For SiO_2@GOAG, the CL intensity suddenly increased when the concentration of IGA3 reached to 5.3×10^{-9} moL/L and the saturated immobilization amount was calculated as 2.75×10^{-8} moL/g according to formula (1). Similarly, the immobilized saturation amounts of GO and Fe_3O_4@SiO_2@GO to IGA3 were calculated as 1.25×10^{-8} moL/g and 1.75×10^{-8} moL/g, respectively. Compared with these results, SiO_2@GOAG exhibited a significantly enhanced immobilization amount. Fig. 6(B) was the equilibrium time curves of GO, Fe_3O_4@SiO_2@GO and SiO_2@GOAG to IGA3. SiO_2@GOAG could easily reach its saturated immobilization amount within 15 min, compared to 30 min of GO and 20 min of Fe_3O_4@SiO_2@GO. By comparison of these data, SiO_2@GOAG exhibited better immobilization kinetics, which attributed to the non-covalent interaction of π-π stacking effect and hydrogen bond between IGA3 and SiO_2@GOAG.

3.4. Combination properties

The combination properties of IGA3/SiO_2@GOAG to ssDNA-AuNPs were researched, including the saturated combination amount and equilibrium time. Fig. 6(C) was the saturated combination amount curve of IGA3/SiO_2@GOAG to ssDNA-AuNPs. The CL intensity suddenly increased when the concentration of ssDNA-AuNPs reached to 5.0×10^{-9} moL/L and the saturated combination amount of IGA3 was calculated as 2.50×10^{-8} moL/g according to formula (2). Fig. 6(D) showed the combination equilibrium time of IGA3/SiO_2@GOAG to ssDNA-AuNPs. The maximum combination amount could be easily reached within 15 min. These superior

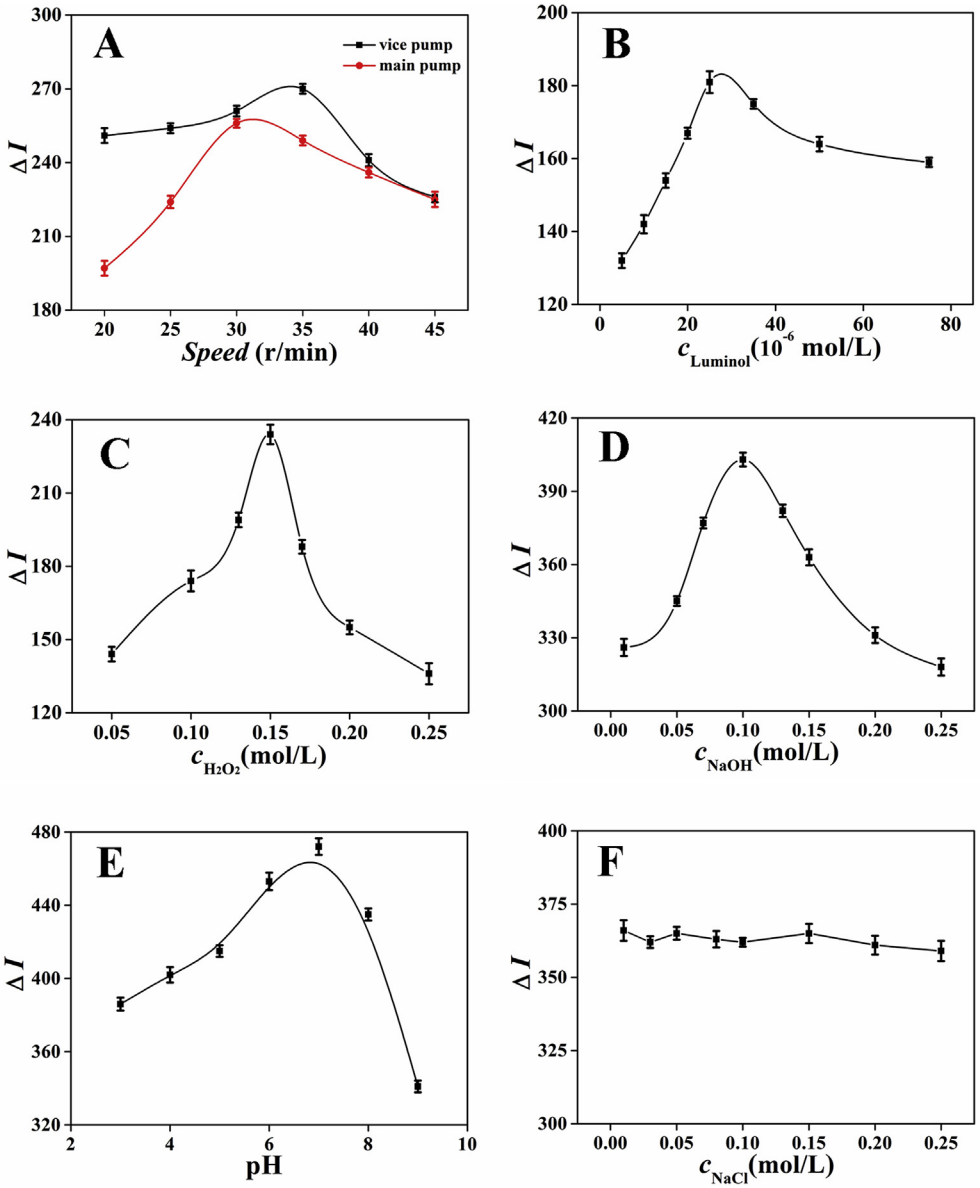

Fig. 7. Optimizations of pumps speed, conditions: 5.0×10^{-5} moL/L luminol, 0.10 moL/L H_2O_2, 0.10 moL/L NaOH and 2.5×10^{-10} moL/L ssDNA-AuNPs (A); the concentration of luminol, conditions: 30 r/min main speed, 35 r/min vice speed, 0.10 moL/L H_2O_2, 0.10 moL/L NaOH and 2.5×10^{-10} moL/L ssDNA-AuNPs (B), the concentration of H_2O_2, conditions: 30 r/min main speed, 35 r/min vice speed, 2.5×10^{-5} moL/L luminol, 0.10 moL/L NaOH and 2.5×10^{-10} moL/L ssDNA-AuNPs (C), the concentration of NaOH, conditions: 30 r/min main speed, 35 r/min vice speed, 2.5×10^{-5} moL/L luminol, 0.15 moL/L H_2O_2 and 2.5×10^{-10} moL/L ssDNA-AuNPs (D); the pH of solution, conditions: 30 r/min main speed, 35 r/min vice speed, 2.5×10^{-5} moL/L luminol, 0.15 moL/L H_2O_2, 0.10 moL/L NaOH and 2.5×10^{-10} moL/L ssDNA-AuNPs (E); the ionic strength of solution, conditions: 30 r/min main speed, 35 r/min vice speed, 2.5×10^{-5} moL/L luminol, 0.15 moL/L H_2O_2, 0.10 moL/L NaOH and 2.5×10^{-10} moL/L ssDNA-AuNPs (F) of the CL biosensor, (Error bar of all graphs: $n = 6$).

properties were attributed to base pairing interactions between IGA3 of IGA3/SiO_2@GOAG and ssDNA of ssDNA-AuNPs.

3.5. Optimizations of the CL biosensor

To obtain the optimal CL intensity for insulin detection, the factors could influence the CL intensity were optimized by single variable experiments, including the pumps speed of the flow injection device; the concentrations of luminol, H_2O_2 and NaOH; and the pH and ionic strength in solution. The optimized results were shown in Fig. 7.

The peristaltic pumps speed was an important parameter because it can influence the amount of reagents and the combination amount of IGA3/SiO_2@GOAG to ssDNA-AuNPs, so pumps speed was researched. As shown in Figs. 7(A), 30 rpm of main pump speed and 35 rpm of vice pump speed were selected as the optimal pumps speed. The concentrations of luminol, H_2O_2 and NaOH were also optimized, showed in Fig. 7(B-D). Optimal concentrations were obtained: 0.10 moL/L H_2O_2, 0.05 moL/L NaOH and 7.5×10^{-5} moL/L luminol.

The effect of pH was also researched in the range of pH 3.0 to pH 9.0. As shown in Fig. 7(E), the CL intensity reached a maximum when pH in solution was 7.4. When pH was lower or higher, the CL intensity decreased. This trend could be related to the stability of ssDNA-AuNPs/IGA3/SiO_2@GOAG and its stability was optimal at pH 7.4. Therefore, PBS with pH 7.4 was used to prepare insulin-spiked buffer and dilute insulin samples. The ionic strength could affect the stability of nucleic acids and in turn affected the binding of

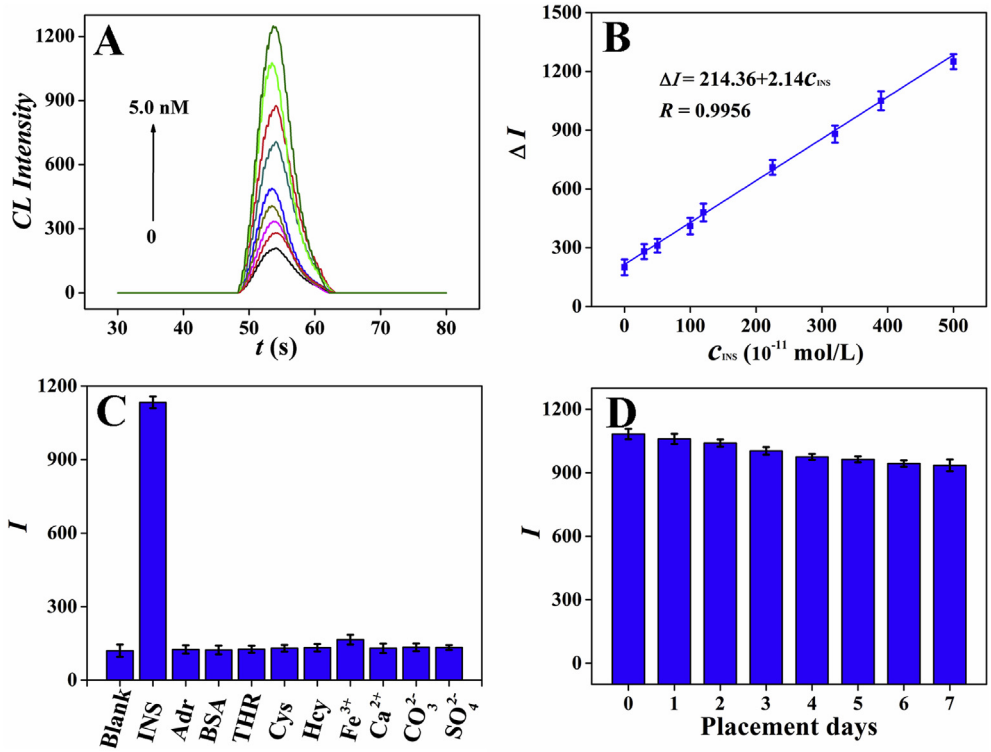

Fig. 8. The CL curves in the presence of different concentrations of insulin (7.5×10^{-12}, 3.0×10^{-11}, 5.0×10^{-11}, 1.0×10^{-10}, 4.5×10^{-10}, 2.2×10^{-9}, 3.2×10^{-9}, 4.0×10^{-9} and 5.0×10^{-9} moL/L) (A); the linear relationship curve of the proposed CL biosensor (B); the relatively CL intensity after incubation with different substances, conditions: 2.0×10^{-11} moL/L insulin (INS), 2.0×10^{-9} moL/L adrenaline (Adr), 2.0×10^{-9} moL/L thrombin (THR), 4.5×10^{-9} moL/L bovine serum albumin (BSA), 4.5×10^{-9} moL/L cystine (Cys), 4.5×10^{-9} moL/L homocysteine (Hcy), 2.0×10^{-7} moL/L Fe^{3+}, 2.0×10^{-7} moL/L Ca^{2+}, 2.0×10^{-7} moL/L CO_3^{2-} and 2.0×10^{-7} moL/L SO_4^{2-}(C); the stability study of sample containing ssDNA-AuNPs/IGA3/SiO_2@GOAG placed in different days (D) (Error bar of all graphs: $n = 6$).

Table 1
Comparisons with some reported methods.

Method	Linear range (mol/L)	Detection limit (mol/L)
Our work[a]	7.5×10^{-12} - 5.0×10^{-9}	1.6×10^{-12}
Electrochemical impedance biosensor [9]	1.0×10^{-9} - 1.0×10^{-6}	2.7×10^{-10}
Flow injection amperometric [10]	5.0×10^{-10} - 1.5×10^{-8}	1.1×10^{-10}
Electrochemiluminescence biosensor [11]	1.7×10^{-14} - 5.2×10^{-9}	5.2×10^{-15}
FL sensor based on aptamer composite [12] [b]	4.3×10^{-9} - 2.1×10^{-7}	2.74×10^{-9}
Label-free sensor based on SERS [14] [a]	1.0×10^{-10} - 5.0×10^{-8}	3.5×10^{-11}
Photoelectrochemical immunosensor [15]	1.7×10^{-12} - 3.4×10^{-9}	3.4×10^{-13}
LC-MS/MS assay [61] [a]	1.8×10^{-11} - 1.9×10^{-9}	1.8×10^{-11}
Quartz crystal microbalance [62]	1.4×10^{-12} - 1.7×10^{-9}	2.7×10^{-13}
Electrochemical sensor [63] [c]	2.0×10^{-8} - 1.0×10^{-6}	5.0×10^{-9}
Electrochemical aptamer-based sensor [64]	1.0×10^{-8} - 2.0×10^{-7}	1.0×10^{-8}

[a] Human recombinant insulin.
[b] Insulin from bovine pancreas.
[c] Porcine insulin.

Table 2
Recoveries for insulin detection in insulin injection.

Sample	C_{added} (10^{-10} moL/L)	C_{found} (10^{-10} moL/L, $n = 6$)	RSD (%)	Recovery (%)
1	1.0	0.98	1.84	98.0
2	3.0	3.01	2.26	100.3
3	5.0	4.97	1.93	99.4
4	8.0	7.96	1.63	99.5
5	10.0	10.06	2.82	100.6

aptamers to targets, so the effect of ionic strength was researched and NaCl with different concentrations was added to PBS. Fig. 7(F) showed the CL intensity slightly changed with the concentration of NaCl, and it was because the ionic strength in the detection system with a large amount of sodium ions, phosphate ions, hydroxide ions, etc. and the single-stranded nucleotide chain had good stability. The intermediate concentration (0.15 moL/L) was selected as the optimal ionic strength.

Table 3
Validation experiments of the proposed CL biosensor.

Sample	C_{added} (10^{-10} moL/L)	C_{found} (10^{-10} moL/L, n = 6)	RSD (%)	Recovery (%)
1	3.00	2.95	1.68	98.3
2	5.00	5.04	2.74	100.8
3	8.00	7.98	1.66	99.7
1′	3.00	3.04	2.15	101.3
2′	5.00	4.93	1.62	98.6
3′	8.00	8.07	2.23	100.8

1, 2, 3 samples were detected by our proposed method and insulin injection was detected after 50 times of dilution; 1′, 2′, 3′samples were detected by HPLC and insulin injection was detected after 100 times of dilution.

3.6. Analytical performances of the CL biosensor

Under optimal conditions, analytical performances of the proposed CL biosensor were researched. Fig. 8(A) was the CL spectrum curves under different concentrations of insulin and a test is completed in only 55 s when the sample has been introduced to the sensor. It showed that the CL intensity gradually increased with the concentration of insulin. Fig. 8(B) showed a good linear correlation between CL intensity (ΔI) and the concentration of insulin (c_{INS}) in the range of 7.5×10^{-12} to 5.0×10^{-9} moL/L. The regression equation was $\Delta I = 214.36 + 2.14\ c_{INS}$ (c_{INS}: 10^{11} moL/L, $R = 0.9956$) and the detection limit was 1.6×10^{-12} moL/L (S/N = 3) for insulin detection.

The proposed CL biosensor to detect insulin was also contrasted with some reported methods, shown in Table 1. By comparison, our proposed CL biosensor showed a relatively wide linear range and low detection limit for insulin detection. The lower detection limit can be attributed to the excellent catalytic performance of ssDNA-AuNPs. Though some of mentioned methods had higher sensitivity and wider linear ranges than our method, the proposed biosensor showed more advantages as follows: the samples and the synthetic composite were oscillated and mixed directly without complicated pretreatment; the test solution entering the detection cell was more easily separated with tweezers than with static or magnetic separation; and automatically injection was easily achieved by a flow injection device. Therefore, the proposed biosensor provided a convenient method for insulin detection. However, the proposed detection method is not yet portable. The defect can be compensated by combining microfluidics, paper chips, etc., and we will make efforts in the follow-up work.

3.7. Specificity, stability and reproducibility of the CL biosensor

Interference experiments were carried out to measure the selectivity of proposed CL biosensor. Interfering substances included several general biological molecules such as adrenaline (Adr), bovine serum albumin (BSA), thrombin (THR), L-cystine (Cys) and homocysteine (Hcy), and some common ions such as Fe^{3+}, Ca^{2+}, CO_3^{2-} and SO_4^{2-}. As shown in Fig. 8(C), the insulin sample showed a high CL intensity while the CL intensity of different interferences were comparable to the control group (Blank). These results demonstrated that the proposed CL biosensor had a high selectivity for insulin detection, which was attributed to the high biorecognition and binding abilities between the aptamers and targets. A nonspecific aptamer (N-Apt) was introduced as a control group to verify the excellent selectivity of the biosensor. The CL intensity of N-Apt was lower than that of IGA3 and comparable to that of the control group that without IGA3 and N-Apt (Fig. S2). The results were because N-Apt could not bind to the target molecule (insulin molecule) and ssDNA-AuNPs was not released, so the CL intensity was weak.

To evaluate the stability of the biosensor, the sample tubes were stored at 4 °C for 1 week. The CL intensity at different storage time was determined, shown in Fig. 8(D). The results showed that the CL intensity remained at about 90.9% of the original intensity after 1 week, which verified good stability of the biosensor. The repeatability of the CL biosensor was also studied by determining the CL response of 11 insulin samples with the same concentration (5.0×10^{-10} moL/L). The relative standard deviation (RSD) was about 1.28%, which indicated the acceptable repeatability of the proposed biosensor.

3.8. Applications of the CL biosensor

Under the optimal conditions, the proposed biosensor was used for insulin detection in insulin injection. The insulin injection was diluted 100 times with PBS in advance. The above diluted 0.5 mL insulin injection and a certain amount of standard insulin (1.0×10^{-10}, 3.0×10^{-10}, 5.0×10^{-10}, 8.0×10^{-10} and 1.0×10^{-9} moL/L) were added to sample tubes for recovery experiments. As shown in Table 2, the spiked recoveries were of 98.0%–100.6% and RSD was less than 2.82%, which indicated the good accuracy and precision for insulin detection. These satisfactory results demonstrated that the proposed CL biosensor had a good potential application in the detection of insulin in insulin injections.

Validation experiments were carried out to further confirm the accuracy of the proposed method. Under optimized conditions, parallel insulin injection samples were tested by our developed method and generally accepted HPLC method, and these results were shown in Table 3. Obviously, these results showed the proposed method were consistent with that of HPLC. The recoveries of our method were in the range of 98.3%–100.8% while that of HPLC method were of 98.6%–101.3%. These results further verified the good application prospects of the CL biosensor.

4. Conclusions

In summary, the multi-functionalized ssDNA-AuNPs/IGA3/SiO_2@GOAG was successfully prepared and used for the construction of CL biosensor for insulin detection. IGA3 was a biorecognition element and improved the selectivity of the CL biosensor. ssDNA-AuNPs was a catalyst for luminol-H_2O_2 and improved the sensitivity of the CL biosensor. Under the optimal conditions, the CL biosensor for insulin detection showed a wide linear concentration range of 7.5×10^{-12} to 5.0×10^{-9} moL/L and low detection limit of 1.6×10^{-12} moL/L (S/N = 3). Finally it was successfully used for insulin detection in insulin injection samples and the recoveries were in range of 98.0%–103.3%. So the proposed CL biosensor could be further used in the product prosecution of insulin injections.

Declaration of competing interest

The authors declare that they have no known competing financial interests or personal relationships that could have appeared to influence the work reported in this paper.

Acknowledgements

This work was supported by National Science Foundation for Young Scientists of China (No. 21605094), Youth Science fund of Shandong Academy of Sciences (No. 2017QN006), Shandong Province Natural Science Institute Joint Fund (No. ZR2015YL006), Shandong Provincial Natural Science Foundation of China (No. ZR2016BM01) and Horizontal Scientific Research Project of China (No. W15077).

Appendix A. Supplementary data

Supplementary data to this article can be found online at https://doi.org/10.1016/j.aca.2019.09.004.

References

[1] K.G.M.M. Alberti, P.Z. Zimmet, Definition, diagnosis and classification of diabetes mellitus and its complications. Part 1: diagnosis and classification of diabetes mellitus provisional report of a WHO consultation, Diabet. Med. 15 (7) (1998) 539–553.
[2] N. Sneha, T. Gangil, Analysis of diabetes mellitus for early prediction using optimal features selection, Journal of Big Data 6 (1) (2019) 1–19.
[3] R. Soffe, V. Nock, J.G. Chase, Towards point-of-care insulin detection, ACS Sens. 4 (2019) 3–19.
[4] G. Jia, V. DeMarco, J.R. Sowers, Insulin resistance and hyperinsulinaemia in diabetic cardiomyopathy, Nat. Rev. Endocrinol. 12 (3) (2016) 144–153.
[5] S. Tony, Diabetes in numbers, Nature 485 (2013) S2–S3.
[6] J.G. Chase, G.M. Shaw, J. Lin, C.V. Doran, C. Hann, et al., Targeted glycemic reduction in critical care using closed-loop control, Diabetes Technol. Ther. 7 (2) (2005) 274–282.
[7] J.G. Chase, G. Shaw, A.L. Compte, T. Lonergan, M. Willacy, X. Wong, et al., Implementation and evaluation of the SPRINT protocol for tight glycaemic control in critically ill patients: a clinical practice change, Crit. Care 12 (2) (2008). R49-R49.
[8] M. Blackburn, Advances in the quantitation of therapeutic insulin analogues by LC-MS/MS, Bioanalysis 5 (23) (2013) 2933–2946.
[9] A.A. Ensafi, E. Khoddami, B. Rezaei, Aptamer@Au-o-phenylenediamine modified pencil graphite electrode: a new selective electrochemical impedance biosensor for the determination of insulin, Colloids Surfaces B Biointerfaces 159 (2017) 47–53.
[10] E. Habibi, E. Omidinia, H. Heidari, M. Fazli, Flow injection amperometric detection of insulin at cobalt hydroxide nanoparticles modified carbon ceramic electrode, Anal. Biochem. 495 (2016) 37–41.
[11] W. Zhu, C. Wang, X. Li, M.S. Khan, X. Sun, et al., Zinc-doping enhanced cadmium sulfide electrochemiluminescence behavior based on Au-Cu alloy nanocrystals quenching for insulin detection, Biosens. Bioelectron. 97 (2017) 115–121.
[12] J. Yang, Z. Zhang, G. Yan, An aptamer-mediated CdSe/ZnS QDs@graphene oxide composite fluorescent probe for specific detection of insulin, Sens. Actuators B Chem. 255 (2017) 2339–2346.
[13] S. Dong, Y. Zeng, G. Wei, D. Si, C. Liu, Determination of human insulin in dog plasma by a selective liquid chromatography-tandem mass spectrometry method: application to a pharmacokinetic study, J. Chromatogr. B 1077 (2018) 85–91.
[14] H. Cho, S. Kumar, D. Yang, S. Vaidyanathan, K. Woo, et al., Surface-enhanced Raman spectroscopy-based label-free insulin detection at physiological concentrations for analysis of islet performance, ACS Sens. 3 (2018) 65–71.
[15] D. Fan, H. Wang, M.S. Khan, C. Bao, H. Wang, et al., An ultrasensitive photoelectrochemical immunosensor for insulin detection based on BiOBr/Ag_2S composite by in-situ growth method with high visible-light activity, Biosens. Bioelectron. 97 (2017) 253–259.
[16] B. Heurtault, N. Reix, N. Meyer, F. Gasser, M.J. Wendling, et al., Extensive study of human insulin immunoassays: promises and pitfalls for insulin analogue detection and quantification, Clin. Chem. Lab. Med. 52 (3) (2014) 355–362.
[17] N. Siraj, B. El-Zahab, S. Hamdan, T.E. Karam, L.H. Haber, et al., Fluorescence, phosphorescence, and chemiluminescence, Anal. Chem. 88 (1) (2015) 170–202.
[18] P. Yao, Z. Liu, S. Tung, Z. Dong, L. Liu, Fully automated quantification of insulin concentration using a microfluidic-based chemiluminescence immunoassay, J. Lab. Autom. 21 (3) (2016) 387–393.
[19] H. Ma, X. Li, T. Yan, Y. Li, H. Liu, et al., Sensitive insulin detection based on electrogenerated chemiluminescence resonance energy transfer between $Ru(bpy)_3^{2+}$ and Au nanoparticle-doped beta-Cyclodextrin-Pb (II) metal-organic framework, ACS Appl. Mater. Interfaces 816 (2016) 10121–10127.
[20] M. Liu, Z. Wang, C. Zhang, Recent advance in chemiluminescence assay and its biochemical applications, Chin. J. Anal. Chem. 44 (12) (2016) 1934–1941.
[21] Q. Xiao, J. Lin, Advances and applications of chemiluminescence immunoassay in clinical diagnosis and foods safety, Chin. J. Anal. Chem. 43 (6) (2015) 929–938.
[22] Y. Lin, Y. Dai, Y. Sun, C. Ding, W. Sun, et al., A turn-on chemiluminescence biosensor for selective and sensitive detection of adenosine based on HKUST-1 and QDs-luminol-aptamer conjugates, Talanta 182 (2018) 116–124.
[23] Y. Sun, C. Ding, Y. Lin, W. Sun, H. Liu, et al., Highly selective and sensitive chemiluminescence biosensor for adenosine detection based on carbon quantum dots catalyzing luminescence released from aptamers functionalized graphene@magnetic β-cyclodextrin polymers, Talanta 186 (2018) 238–247.
[24] W. Cao, Y. Chao, L. Liu, Q. Liu, M. Pei, Flow injection chemiluminescence sensor based on magnetic oil-based surface molecularly imprinted nanoparticles for determination of bisphenol A, Sens. Actuators B Chem. 204 (2014) 704–709.
[25] C.L.A. Hamula, J.W. Guthrie, H. Zhang, X. Li, X. Chris Le, Selection and analytical applications of aptamers, Trends Anal. Chem. 25 (2006) 681–691.
[26] M. McKeague, M.C. DeRosa, Challenges and opportunities for small molecule aptamer development, J. Nucleic Acids 2012 (2012) 1–21.
[27] Y. Wu, F. Nie, D. Xia, Chemiluminescence assay for the glycoprotein tenascin-C based on aptamer-modified carboxylated magnetic carbon nanoparticles, Microchimica Acta 182 (1–2) (2015) 227–232.
[28] S. Shan, Z. He, S. Mao, M. Jie, L. Yi, et al., Quantitative determination of VEGF165 in cell culture medium by aptamer sandwich based chemiluminescence assay, Talanta 171 (2017) 197–203.
[29] Y. Ando, K. Niwa, N. Yamada, T. Irie, T. Enomoto, et al., Development of a quantitative bio/chemiluminescence spectrometer determining quantum yields: Re-examination of the aqueous luminol chemiluminescence standard, Photochem. Photobiol. 83 (5) (2010) 1205–1210.
[30] W. Li, Q. Zhang, H. Zhou, J. Chen, Y. Li, et al., Chemiluminescence detection of a protein through the aptamer-controlled catalysis of a porphyrin probe, Anal. Chem. 87 (16) (2015) 8336–8341.
[31] M. Iranifam, Chemiluminescence reactions enhanced by silver nanoparticles and silver alloy nanoparticles: applications in analytical chemistry, Trends Anal. Chem. 82 (2016) 126–142.
[32] J. Yao, L. Li, P. Li, M. Yang, Quantum dots: from fluorescence to chemiluminescence, bioluminescence, electrochemiluminescence, and electrochemistry, Nanoscale 9 (36) (2017) 13364–13383.
[33] X. Liu, R. Freeman, E. Golub, I. Willner, Chemiluminescence and chemiluminescence resonance energy transfer (CRET) aptamer sensors using catalytic hemin/G-quadruplexes, ACS Nano 5 (9) (2011) 7648–7655.
[34] X. Hun, Y. Xu, L. Bai, A chemiluminescence assay for L-histidine based on controlled DNAzyme catalytic reactions on magnetic microparticles, Microchimica Acta 182 (3–4) (2015) 565–570.
[35] Z. Zhang, H. Cui, C. Lai, L. Liu, Gold nanoparticle-catalyzed luminol chemiluminescence and its analytical applications, Anal. Chem. 77 (10) (2005) 3324–3329.
[36] N. Li, J. Guo, B. Liu, Y. Yu, H. Cui, et al., Determination of monoamine neurotransmitters and their metabolites in a mouse brain microdialysate by coupling high-performance liquid chromatography with gold nanoparticle-initiated chemiluminescence, Anal. Chim. Acta 645 (2009) 48–55.
[37] Y. Zhang, J. Liu, T. Liu, H. Li, Q. Xue, et al., Label-free, sensitivity detection of fibrillar fibrin using gold nanoparticle-based chemiluminescence system, Biosens. Bioelectron. 77 (2016) 111–115.
[38] H. Chen, Q. Gao, J. Li, J. Lin, Graphene materials-based chemiluminescence for sensing, J. Photochem. Photobiol. C Photochem. Rev. 27 (2016) 54–71.
[39] C. Chen, X. Zhu, B. Chen, Covalently cross-linked graphene oxide aerogel with stable structure for high-efficiency water purification, Chem. Eng. J. 354 (2018) 896–904.
[40] Y. Wang, Y. Jin, C. Zhao, E. Pan, M. Jia, Fe_3O_4 nanoparticle/graphene aerogel composite with enhanced lithium storage performance, Appl. Surf. Sci. 458 (2018) 1035–1042.
[41] R. Li, F. Cui, H. Zhu, X. Sun, Z. Li, Electrochemical sensor for detection of cancer cell based on folic acid and octadecylamine-functionalized graphene aerogel microspheres, Biosens. Bioelectron. 119 (2018) 156–162.
[42] M. Arabi, M. Ghaedi, A. Ostovan, Development of dummy molecularly imprinted based on functionalized silica nanoparticles for determination of acrylamide in processed food by matrix solid phase dispersion, Food Chem. 210 (2016) 78–84.
[43] S.A. Mahadik, F. Pedraza, R.S. Vhatkar, Silica based superhydrophobic coating for long-term industrial and domestic applications, J. Alloy. Comp. 663 (2016) 487–493.
[44] M.K. Gangishetty, K.E. Lee, R.W.J. Scott, T.L. Kelly, Plasmonic enhancement of dye sensitized solar cells in the red-to-near-infrared region using triangular core-shell Ag@SiO_2 nanoparticles, Applied Materials & Interfaces 5 (21) (2013) 11044–11051.
[45] S. Zhang, Z. Chu, C. Yin, G. Lin, Q. Li, Controllable drug release and simultaneously carrier decomposition of SiO_2-drug composite nanoparticles, J. Am. Chem. Soc. 135 (15) (2013) 5709–5716.
[46] K. Wang, P. Liu, Y. Ye, J. Li, W. Zhao, et al., Fabrication of a novel laccase biosensor based on silica nanoparticles modified with phytic acid for sensitive detection of dopamine, Sens. Actuators B Chem. 197 (2014) 292–299.
[47] Z. Chen, Y. Tan, K. Xu, L. Zhang, B. Qiu, et al., Stimulus-response mesoporous silica nanoparticle-based chemiluminescence biosensor for cocaine determination, Biosens. Bioelectron. 75 (2016) 8–14.
[48] W. Zhu, C. Xuan, G. Liu, Z. Chen, W. Wang, A label-free fluorescent biosensor for determination of bovine serum albumin and calf thymus DNA based on gold nanorods coated with acridine orange-loaded mesoporous silica, Sens. Actuators B Chem. 220 (2015) 302–308.
[49] W. Yoshida, E. Mochizuki, M. Takase, H. Hasegawa, Y. Morita, et al., Selection

of DNA aptamers against insulin and construction of an aptameric enzyme subunit for insulin sensing, Biosens. Bioelectron. 24 (5) (2009) 1116–1120.
[50] Y. Sun, Y. Lin, C. Ding, W. Sun, Y. Dai, et al., An ultrasensitive and ultraselective chemiluminescence aptasensor for dopamine detection based on aptamers modified magnetic mesoporous silica @ graphite oxide polymers, Sens. Actuators B Chem. 257 (2018) 312–323.
[51] Y. Wong, L. Zhu, W. Teo, Y. Tan, Y. Yang, et al., Revisiting the stober method: in homogeneity in silica shells, J. Am. Chem. Soc. 133 (30) (2011) 11422–11425.
[52] M. Wu, R. Kempaiah, P.J.J. Huang, V. Maheshwari, J. Liu, Adsorption and desorption of DNA on graphene oxide studied by fluorescently labeled oligonucleotides, Langmuir 27 (6) (2011) 2731–2738.
[53] Y. Xu, Q. Wu, Y. Sun, H. Bai, G. Shi, Three-dimensional self-assembly of graphene oxide and DNA into multifunctional hydrogels, ACS Nano 4 (12) (2010) 7358–7362.
[54] B. Niu, Y. Zhou, T. Wen, G. Quan, V. Singh, et al., Proper functional modification and optimized adsorption conditions improved the DNA loading capacity of mesoporous silica nanoparticles, Colloid. Surf. Physicochem. Eng. Asp. 548 (2018) 98–107.
[55] D.C. Marcano, D.V. Kosynkin, J.M. Berlin, A. Sinitskii, Z. Sun, et al., Improved synthesis of graphene oxide, ACS Nano 4 (8) (2010) 4806–4814.
[56] Q. Guo, G. Yang, D. Huang, W. Cao, L. Ge, et al., Synthesis and characterization of spherical silica nanoparticles by modified Stöber process assisted by slow-hydrolysis catalyst, Colloid Polym. Sci. 296 (2) (2018) 379–384.
[57] L. Du, C. Zhang, L. Wang, G. Liu, Y. Zhang, et al., Ultrasensitive time-resolved microplate fluorescence immunoassay for bisphenol A using a system composed on gold nanoparticles and a europium(III)-labeled streptavidin tracer, Microchim Acta 182 (2015) 539–545.
[58] E.E. Connor, J. Mwamuka, A. Gole, C.J. Murphy, M.D. Wyatt, Gold nanoparticles are taken up by human cells but do not cause acute cytotoxicity, Small 1 (2015) 325–327.
[59] Z. Liu, F. Zhao, S. Gao, J. Shao, H. Chang, The applications of gold nanoparticle initialed chemiluminescence in biomedical detection, Nanoscale Research Letters 11 (2016) 460–467.
[60] Y. Sun, J. Li, Y. Wang, C. Ding, Y. Lin, et al., A chemiluminescence biosensor based on the adsorption recognition function between Fe_3O_4@SiO_2@GO polymers and DNA for ultrasensitive detection of DNA, Spectrochim. Acta A Mol. Biomol. Spectrosc. 178 (2017) 1–7.
[61] A. Thomas, P.T. Brinkkotter, W. Schanzer, M. Thevis, Simultaneous determination of insulin, DesB30 insulin, proinsulin, and C-peptide in human plasma samples by liquid chromatography coupled to high resolution mass spectrometry, Forensic Toxicol. 35 (2017) 106–113.
[62] F. Kartal, D. Çimen, N. Bereli, A. Denizli, Molecularly imprinted polymer based quartz crystal microbalance sensor for the clinical detection of insulin, Mater. Sci. Eng. C 97 (2019) 730–737.
[63] C. Guo, C. Chen, Z. Luo, L. Chen, Electrochemical behavior and analytical detection of insulin on pretreated nanocarbon black electrode surface, Analytical Methods 4 (5) (2012) 1377–1382.
[64] J.Y. Gerasimov, C.S. Schaefer, W. Yang, R.L. Grout, R.Y. Lai, Development of an electrochemical insulin sensor based on the insulin-linked polymorphicregion, Biosens. Bioelectron. 42 (2013) 62–68.